Multiparametric photoacoustic microscopy of the mouse brain with 300-kHz A-line rate

Tianxiong Wang
Naidi Sun
Rui Cao
Bo Ning
Ruimin Chen
Qifa Zhou
Song Hu

Multiparametric photoacoustic microscopy of the mouse brain with 300-kHz A-line rate

Tianxiong Wang,[a] **Naidi Sun,**[a] **Rui Cao,**[a] **Bo Ning,**[a] **Ruimin Chen,**[b] **Qifa Zhou,**[b] **and Song Hu**[a,*]
[a]University of Virginia, Department of Biomedical Engineering, 415 Lane Road, Charlottesville, Virginia 22908, United States
[b]University of Southern California, Department of Biomedical Engineering, 1042 Downey Way, Los Angeles, California 90089, United States

Abstract. Enabling simultaneous high-resolution imaging of the total concentration of hemoglobin (C_{Hb}), oxygen saturation of hemoglobin (sO_2), and cerebral blood flow (CBF), multiparametric photoacoustic microscopy (PAM) holds the potential to quantify the cerebral metabolic rate of oxygen at the microscopic level. However, its imaging speed has been severely limited by the pulse repetition rate of the dual-wavelength photoacoustic excitation and the scanning mechanism. To address these limitations, we have developed a new generation of multiparametric PAM. Capitalizing on a self-developed high-repetition dual-wavelength pulsed laser and an optical–mechanical hybrid-scan configuration, this innovative technique has achieved an unprecedented A-line rate of 300 kHz, leading to a 20-fold increase in the imaging speed over our previously reported multiparametric PAM that is based on pure mechanical scanning. The performance of the high-speed multiparametric PAM has been examined both *in vitro* and *in vivo*. Simultaneous PAM of microvascular C_{Hb}, sO_2, and CBF in absolute values over a ~3-mm-diameter brain region of interest can be accomplished within 10 min. © 2016 *Society of Photo-Optical Instrumentation Engineers (SPIE)* [DOI: 10.1117/1.NPh.3.4.045006]

1 Introduction

Capable of providing label-free, comprehensive, and quantitative characterization of cerebral hemodynamics at the microscopic level, photoacoustic microscopy (PAM) has attracted increasing attention in neuroimaging.[1] A recent research focus is to combine the multiple PAM-measured hemodynamic parameters—including the total concentration of hemoglobin (C_{Hb}), oxygen saturation of hemoglobin (sO_2), and cerebral blood flow (CBF)—for quantifying the cerebral metabolic rate of oxygen ($CMRO_2$) at the microscopic level.[2,3] To this end, we have developed multiparametric PAM, which enables simultaneous imaging of C_{Hb}, sO_2, and CBF at the same spatial scale.[4] However, the speed of multiparametric PAM has been severely limited by the pulse repetition rate of the dual-wavelength photoacoustic excitation and the scanning mechanism. By employing two commercially available high-repetition single-wavelength lasers with distinct pulse durations (3 ns and 3 ps) and a customized water-immersible microelectromechanical system (MEMS) scanning mirror, Yao et al.[5] have markedly improved the speed of PAM and demonstrated functional imaging of the mouse brain with 100-kHz A-line rate. Although encouraging, this technique is not applicable for microscopic imaging of $CMRO_2$ because CBF—unlike the other two parameters—can only be measured at selected locations. Moreover, the pulse-duration-based measurement of sO_2 requires high-laser pulse energy (>400 nJ) to induce transient saturation in the optical absorption of blood hemoglobin, exceeding the safety limit recommended by the American National Standards Institute.[6]

Here, we report on an implementation of multiparametric PAM with an unprecedented A-line rate of 300 kHz. This technique sticks to the established spectroscopic measurement of sO_2, which requires much lower pulse energy (<100 nJ) than the saturation-based approach. To allow for high-repetition dual-wavelength excitation, we have developed a 300-kHz laser capable of pulse-by-pulse switching between 532 and 558 nm. To boost the imaging speed while retaining the unique capability of simultaneously mapping C_{Hb}, sO_2, and CBF at the microscopic level, we have implemented optical–mechanical hybrid scan to acquire multiple cross-sectional scans (i.e., B-scans) in parallel. The performance of this new generation of multiparametric PAM has been examined in phantoms and the mouse brain.

2 Materials and Methods

2.1 *Experimental Setup*

As shown in Fig. 1, the high-speed multiparametric PAM utilizes an ytterbium-doped fiber laser (GLPM-10-Y13, IPG Photonics; wavelength: 532 nm; pulse repetition rate: tunable between 10 and 300 kHz; and pulse duration: 1.25 ns). The laser beam passes through an electro-optical modulator (EOM; 350-80, Conoptics) and a half-wave plate (HWP; WPH05M-532, Thorlabs) before being expanded by a lens pair (LA1213-A and LA1608-A, Thorlabs). When a high voltage (260 V) is applied to the EOM, the polarization of the incident beam is rotated to the vertical direction by the EOM and HWP. Thus, the expanded beam is reflected by a polarizing beam splitter (PBS; PBS121, Thorlabs) and then coupled through a microscope objective (M-10X, Newport) into a 5-m-long polarization-maintaining single-mode fiber (PM-SMF; F-SPA, Newport) for stimulated Raman
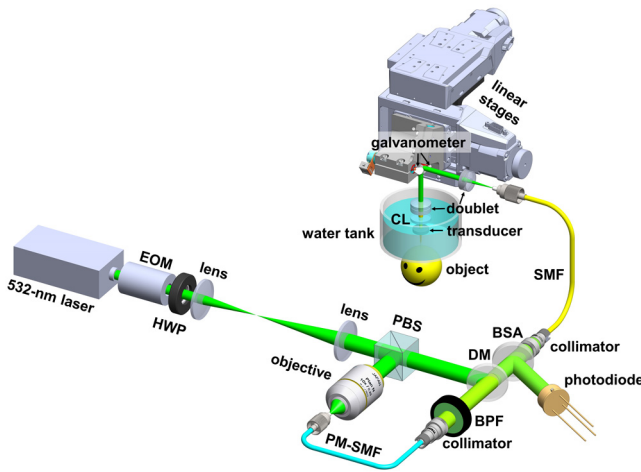
Fig. 1 Schematic of the high-speed multiparametric PAM. EOM, electro-optical modulator; HWP, half-wave plate; PBS, polarizing beam splitter; PM-SMF, polarization-maintaining single-mode fiber; BPF, bandpass filter; DM, dichroic mirror; BSA, beam sampler; SMF, regular single-mode fiber; CL, correction lens.

scattering-based wavelength conversion.[7,8] To maximize the conversion efficiency, the orientation of the PM-SMF is carefully adjusted to align its principal axis with the polarization of the incident light.[9] The output of the PM-SMF is collimated by a collimator (CFC-11X-A, Thorlabs) and purified by a bandpass filter (FB560-10, Thorlabs) to isolate the 558-nm component. When a low voltage (0 V) is applied to the EOM, the 532-nm beam is horizontally polarized after expansion and passes through the PBS without wavelength conversion. Thus, alternating the EOM voltage allows pulse-by-pulse switching of the laser wavelength. The unconverted 532-nm beam and the 558-nm Raman beam are combined via a dichroic mirror (FF538-FDi01, Semrock) and coupled into the imaging head through a 2-m-long regular SMF (P1-460B-FC-2, Thorlabs), before which ∼5% of the combined beam is picked off by a beam sampler (BSF10-A, Thorlabs) and monitored by a high-speed photodiode (FDS100, Thorlabs) to compensate for possible fluctuation in the laser energy. According to our test, the regular SMF with such a short length does not generate noticeable Raman shift to the optical wavelength. In the imaging head, the dual-wavelength beam is collimated by an achromatic doublet (AC127-019-A, Thorlabs), reflected by a two-axis galvanometer scanner (6215HSM40B, Cambridge Technology), and then focused into the object to be imaged by a second doublet (AC127-025-A, Thorlabs) through a correction lens (KPX561, Newport) and the central opening of a customized ring-shaped ultrasonic transducer (inner diameter: 2.0 mm; outer diameter: 4.4 mm; focal length: 5.0 mm; center frequency: 41 MHz; and 6-dB bandwidth: 61%).

The imaging head is mounted on two motorized linear stages (PLS-85, PI miCos) for raster scanning. A homemade water tank is used to immerse the transducer and the correction lens. A thin layer of ultrasound gel (Aquasonic CLEAR®, Parker Laboratories) is sandwiched between the object to be imaged and the transparent polyethylene membrane at the bottom of the water tank for acoustic coupling. A field-programmable gate array (PCIe-7842R, National Instruments) is used to synchronize the laser, EOM, galvanometer scanner, linear stages, and waveform digitizer (ATS9350, AlazarTech) during image acquisition.

2.2 Scanning Mechanism and Measurement Principle

Recent advances have led to dramatic improvements in the speed of PAM,[5,10] but none of them permit CBF mapping at the microscopic level. The multiparametric PAM provides a solution;[4] however, the correlation-based CBF quantification limits its B-scan rate to ∼1 mm/s. To boost the speed of PAM while maintaining the slow B-scan rate for the CBF measurement, we adopted the synchronized one-dimensional optical and two-dimensional (2-D) mechanical hybrid scan.[11] As shown in Fig. 2(a), the galvanometer scanner steers the laser spot along the Y-axis within the acoustic focus of the transducer at a round-trip rate of 2.1 kHz as the linear stage mechanically translates the optical-acoustic dual foci along the X-axis at a constant speed of 0.88 mm/s, during which the laser output is switched between 532 and 558 nm at a 3.3-μs interval to produce dual-wavelength A-line pairs. The optical–mechanical hybrid scan forms a sinusoidal pattern, with 36 pixels acquired at each wavelength in a half cycle. To assure a roughly constant pixel size along the Y-axis, for each wavelength, only the 20 pixels near the center of the optical scan are extracted for image reconstruction. Thus, 20 dual-wavelength B-scans can be simultaneously acquired, leading to a 20-fold increase in the imaging speed over our previously reported multiparametric PAM, which is based on pure mechanical scanning.[4]

Simultaneous mapping of CBF, C_{Hb}, and sO_2 at the microscopic level is realized by correlation, statistical, and spectral analyses of individual B-scans.[4] Specifically, PAM is insensitive to sO_2 at 532 nm, a near-isosbestic point of hemoglobin. Fluctuations in the PAM signal acquired at this wavelength encode both the flow and Brownian motion of red blood cells (RBCs).[12] The speed of CBF is quantified by the decorrelation rate of successively acquired A-lines. Theoretically, the correlation coefficient between two adjacent A-lines depends on their time interval.[13] The time dependence follows a second-order exponential decay, of which the decay constant is linearly proportional to the blood flow speed. As shown in Fig. 2(b), CBF can be quantified by fitting the experimentally measured decorrelation curve with the theoretical model. The faster the decay, the higher the speed. Given the 2.1-kHz round-trip rate of the optical scan and the 0.88-mm/s speed of the mechanical scan, 49 A-lines can be acquired when the linear stage travels 10 μm along the B-scan direction. The decorrelation curve is obtained by calculating the correlation coefficients between the central A-line and each of the 48 preceding and subsequent A-lines and the corresponding time delays. This correlation analysis allows CBF quantification at a spatial scale comparable to the average diameter of capillaries. Note that the measured speed is a vector summation of the speed of the linear stage and that of the CBF. The true CBF speed can be derived using the bidirectional scan as $\sqrt{\frac{1}{2}(v_f^2 + v_b^2 - 2v_m^2)}$, in which v_f and v_b are, respectively, the flow speeds measured by the forward and backward scans and v_m is the B-scan speed.[14] Furthermore, the difference between v_f and v_b reveals the direction of the flow.[4] In parallel, C_{Hb} can be derived from the absolute value by analyzing the Brownian motion-induced statistical fluctuation in the amplitudes of the same 49 A-lines, which is known to depend on the number of RBCs within the detection volume of PAM but not on the flow speed.[15] As shown in Fig. 2(c), the higher the C_{Hb}, the larger the A-line amplitude and the higher the fluctuation. By comparing the readouts at both wavelengths
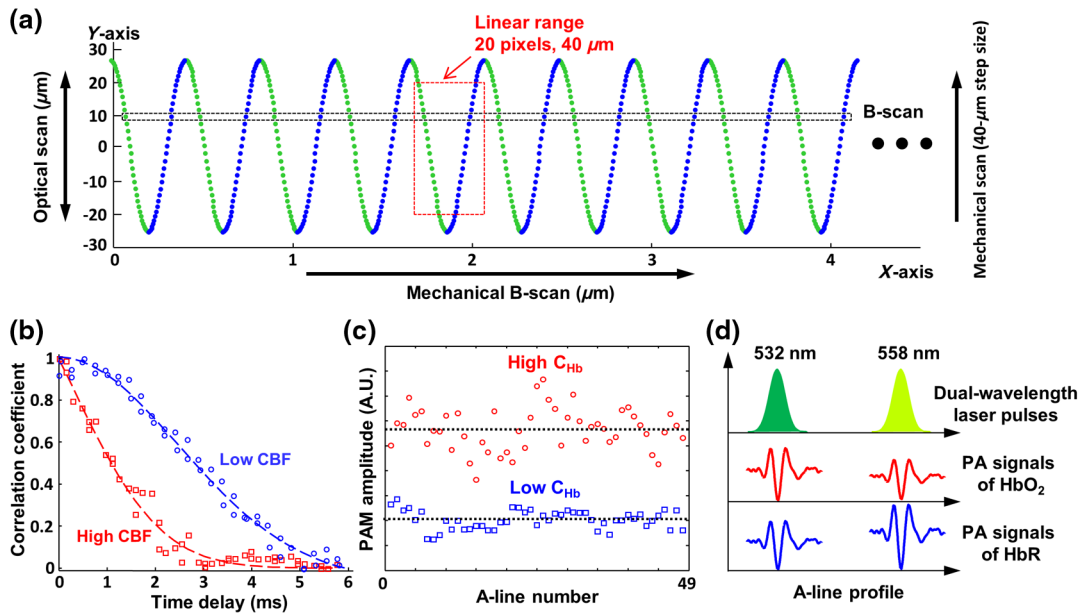
Fig. 2 Scanning mechanism and measurement principle. (a) Scanning scheme of the optical–mechanical hybrid scan. (b)–(d) Correlation, statistical, and spectral analyses of CBF, C_{Hb}, and sO_2, respectively. HbO_2, oxyhemoglobin; HbR, deoxyhemoglobin.

(532 and 558 nm), sO_2 can be simultaneously quantified. As shown in Fig. 2(d), the absorption coefficients of oxy- and deoxyhemoglobin are nearly identical at 532 nm but distinct at 558 nm. Thus, sO_2 can be estimated using spectral decomposition.[16]

2.3 Animal Preparation

A male CD1 mouse (17 weeks old) was used for the *in vivo* study. For optimal imaging quality, the mouse skull above the right somatosensory cortex was thinned to ~100 μm prior to the PAM experiment, forming a circular imaging window with a diameter of ~3 mm. Throughout the PAM experiment, the mouse was maintained under anesthesia with 1.0% to 1.5% isoflurane and the body temperature was kept at 37°C using a temperature-controlled heating pad (EW-89802-52, Cole-Parmer; SRFG-303/10, Omega). All experimental procedures were carried out in conformity with the laboratory animal protocol approved by the Animal Care and Use Committee at the University of Virginia.

3 Results and Discussion

3.1 Stability of the 558-nm Output

In stimulated Raman scattering, the Stokes light has a nonlinear dependence on the pump. Thus, small fluctuations in the 532-nm pump can be amplified when it is Raman shifted. To check the stability of the 558-nm output, we continuously monitored the pulse energy for 660 s and the average power for 120 min using the high-speed photodiode and a power meter (S120C, Thorlabs), respectively. Prior to the monitoring, the coupling efficiency of the 532-nm incident beam to the PM-SMF was maximized and the incident pulse energy was set to 1 μJ, which led to a maximal 558-nm output of 220 nJ. The fluctuation of the room temperature was controlled within 1°C to avoid possible disturbance to the 532-nm laser and the PM-SMF. As shown in Fig. 3, the relative standard deviations of the Raman pulse energy and power were measured to be 0.76% and 1.42%, respectively. Such small fluctuation could be easily compensated for by the high-speed photodiode monitoring during *in vivo* experiments.
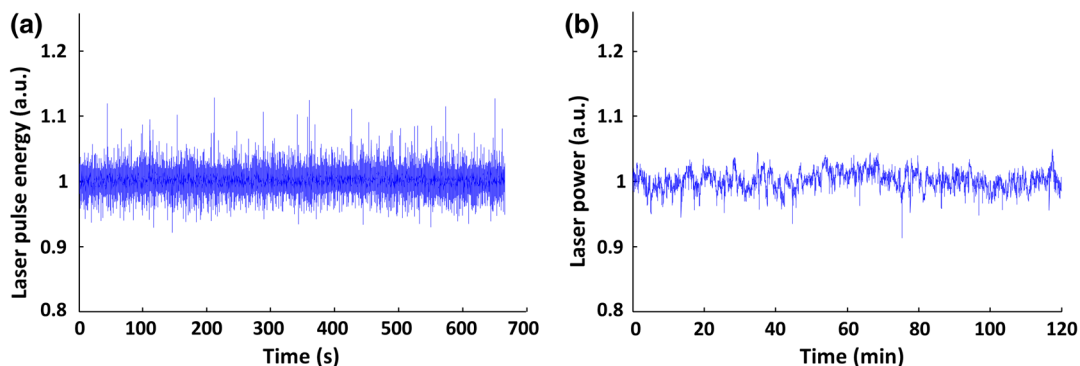
Fig. 3 Stability of the 558-nm Stokes output. (a) Short-term monitoring using high-speed photodiode. (b) Long-term monitoring using power meter.

3.2 Optical Resolution and Acoustic Focal Zone

The optically defined lateral resolution of the multiparametric PAM was examined by imaging a resolution target (R1DS1P, Thorlabs). As shown in Fig. 4(a), the sixth element of Group 7 was clearly resolved. By fitting the experimentally measured modulation transfer function (MTF) to the theoretical MTF of a perfect optical system,[17] we estimated the cutoff spatial frequency to be 259.7 line pair/mm, which corresponded to a lateral resolution of 3.9 μm.

For the optical–mechanical hybrid scan, the optical scanning must be confined within the focal zone of the ultrasonic transducer to ensure sufficient signal-to-noise ratio. The acoustic focus in the transverse plane was experimentally characterized by 2-D optical scanning of a homogeneous black tape over an area of 65 μm by 65 μm. As shown in Fig. 4(b), the circular region with high-photoacoustic amplitudes corresponded to the acoustic focal zone. Gaussian fitting of the cross-sectional profiles [dashed lines in Fig. 4(b)] revealed the acoustic focal diameters along the X- and Y-axis to be 45 and 39 μm, respectively [Fig. 4(c)]. Thus, the voltage applied to the galvanometer scanner was carefully adjusted to spread the 20 pixels over the 40-μm range of optical scanning. It is worth noting that the non-uniform detection sensitivity within the 40-μm acoustic focal zone, as shown in Figs. 4(b) and 4(c), was mathematically compensated for before the quantification of C_{Hb}, sO_2, and CBF.

3.3 Measurable Flow Range

The measurable flow range of the multiparametric PAM is code-termined by the pulse repetition rate of the laser and the B-scan rate.[14] Before, *in vivo* applications, this range was examined in a
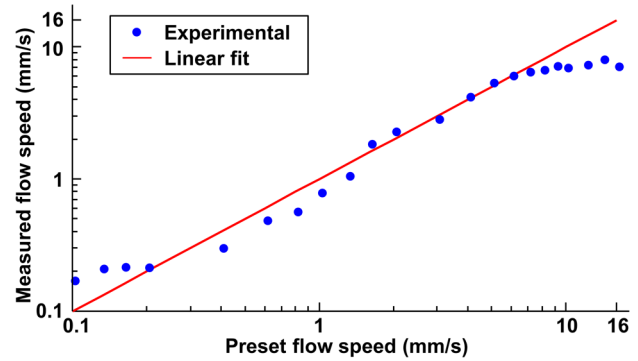

Fig. 5 Examination of the measurable flow range in blood phantom.

vessel-mimicking phantom.[14,18] Specifically, deliberated bovine blood (910, Quad Five) in a plastic tube (56514, United States Plastic Corporation) was driven to flow at 22 different preset speeds by a syringe pump (NE-300, Pump System). The flow speeds of the bovine blood were measured by the high-speed multiparametric PAM and compared with the preset values. Linear regression analysis revealed a strong linear relationship ($R^2 = 0.98$) between the measured and preset flow speeds within the range of 0.2 to 8 mm/s (Fig. 5).

Similar to our previous multiparametric PAM,[14] the upper limit of the measurable flow range is determined by the time interval between two contiguous A-lines in the same B-scan. The smaller the interval, the faster the decorrelation it can sample for the correlation analysis. In our current high-speed multiparametric PAM system, the average interval is ~0.24 ms due to the 2.1-kHz round-trip rate of the galvanometer scanner. This
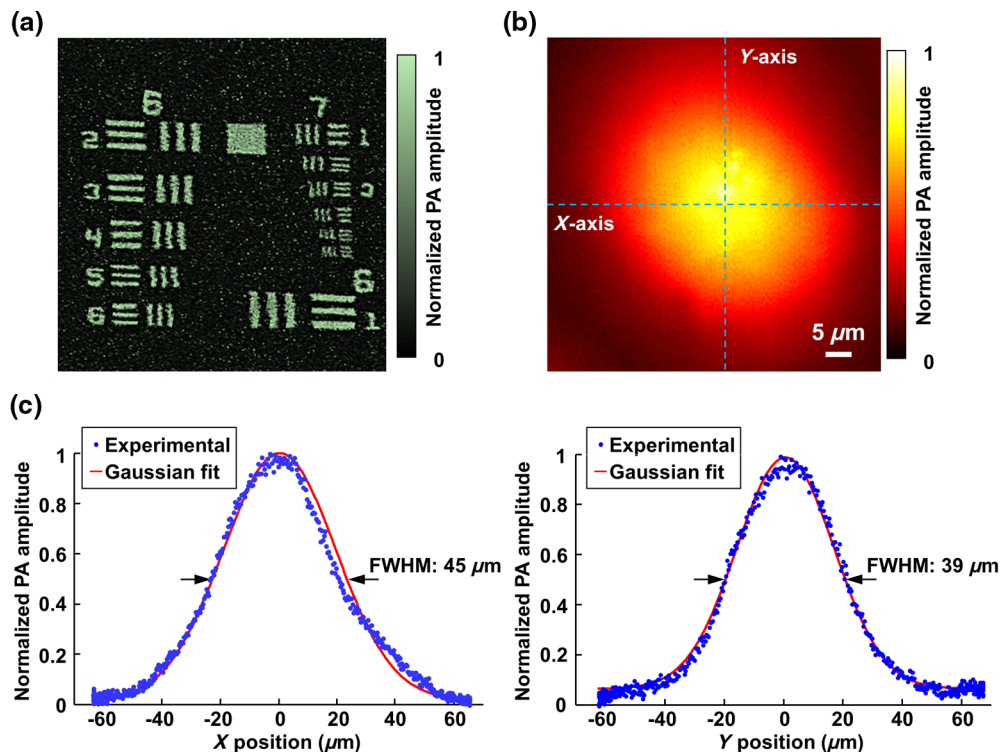

Fig. 4 Optical resolution and acoustic focal zone. (a) Optically defined lateral resolution quantified using a resolution target. (b) Acoustic focal zone within the horizontal plane delineated by 2-D optical scanning of a black tape. (c) Acoustic focal diameters along the X- and Y-axis quantified by the full-width at half-maximum (FWHM) values of the Gaussian-fitted cross-sectional profiles.
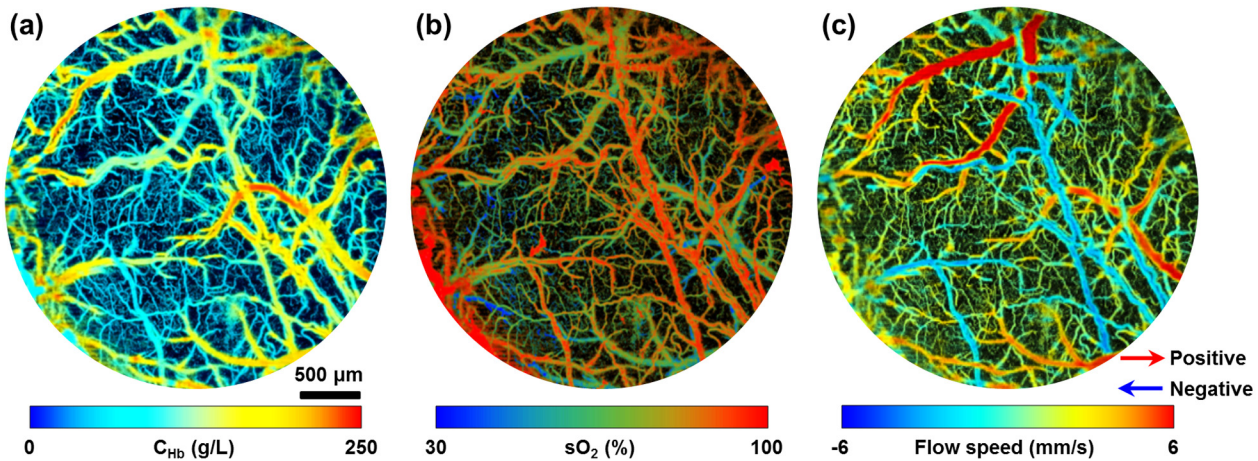
Fig. 6 Simultaneous high-speed PAM of (a) C_{Hb}, (b) sO_2, and (c) CBF (both speed and direction) in the mouse brain.

upper limit can be readily improved using a resonant galvanometer scanner, whose round-trip rate is as high as 12 kHz (e.g., 6SC12KA040-04Y, Cambridge Technology). With that, we can push the limit to ∼50 mm/s. The lower limit is determined by the 5.7-ms correlation window, as shown in Fig. 2(b). The time window is not wide enough to fully record slow decays induced by extremely low speeds. This lower limit can be extended by reducing the B-scan rate at the expense of the imaging time.

3.4 High-Speed Multiparametric Photoacoustic Microscopy of the Mouse Brain In Vivo

Upon examining the performance of the high-speed multiparametric PAM *in vitro*, we further tested its *in vivo* performance in the mouse brain. As shown in Fig. 6, the C_{Hb}, sO_2, and CBF of individual microvessels were simultaneously imaged over a ∼3-mm-diameter cortical region through the thinned-skull window. The pulse energies applied to the mouse brain were 85 and 95 nJ at 532 and 558 nm, respectively. The total image acquisition time was ∼10 min.

The imaging speed of the hybrid scan-based multiparametric PAM is currently limited by the acoustic focal zone and is insufficient to visualize rapid CBF changes in response to the brain stimulation. Within the 40-μm focal diameter, 20 dual-wavelength B-scans are acquired with an average interval of 2 μm, which is much smaller than the 10-μm B-scan interval used in our previous multiparametric PAM and the MEMS-based high-speed PAM.[4,5] Expanding the focal diameter along the *Y*-axis to 200 μm by a cylindrically focused transducer will allow us to spread the 20 B-scans with a 10-μm interval, thereby improving the speed by fivefold. Also, the correlation-based CBF measurement limits the B-scan rate to 0.88 mm/s. In applications where only vascular anatomy and sO_2 are of interest, the B-scan rate can be increased to 10 mm/s, which can further improve the imaging speed by an order of magnitude.

The axial resolution of the reported system is currently limited by the bandwidth of the ultrasonic transducer to ∼50 μm. It cannot resolve overlapping vessels within this focal zone, which may affect the accuracy of the hemodynamic readouts. This limitation can be addressed by increasing the bandwidth of the ultrasonic detection.[19,20]

4 Conclusion

We have developed a new generation of multiparametric PAM with an unprecedented A-line rate of 300 kHz. By integrating the high-repetition dual-wavelength Raman laser and the optical–mechanical hybrid scan, this technology innovation enables simultaneous high-resolution PAM of C_{Hb}, sO_2, and CBF at a speed 20 times faster than that of the previous generation. Expanding the focal zone of the acoustic detection is expected to improve the imaging speed by another fivefold. Envisioned applications of this technique include longitudinal monitoring of hemodynamic and metabolic dysfunctions in ischemic stroke, traumatic brain injury, and Alzheimer's disease.

Disclosures

No conflicts of interest, financial or otherwise, are declared by the authors.

References

1. S. Hu and L. V. Wang, "Neurovascular photoacoustic tomography," *Front. Neuroenerg.* **2**, 10 (2010).
2. L. V. Wang and S. Hu, "Photoacoustic tomography: in vivo imaging from organelles to organs," *Science* **335**(6075), 1458–1462 (2012).
3. S. Hu, "Listening to the brain with photoacoustics," *IEEE J. Sel. Top. Quantum Electron.* **22**(3), 6800610 (2016).
4. B. Ning et al., "Ultrasound-aided multi-parametric photoacoustic microscopy of the mouse brain," *Sci. Rep.* **5**, 18775 (2015).
5. J. Yao et al., "High-speed label-free functional photoacoustic microscopy of mouse brain in action," *Nat. Methods* **12**(5), 407–410 (2015).
6. Laser Institute of America, *American National Standard for Safe Use of Lasers*, ANSI Z136.1-2007, American National Standards Institute, Inc., (2007).
7. P. Hajireza, A. Forbrich, and R. Zemp, "In-vivo functional optical-resolution photoacoustic microscopy with stimulated Raman scattering fiber-laser source," *Biomed. Opt. Express* **5**(2), 539–546 (2014).
8. P. Hajireza, A. Forbrich, and R. J. Zemp, "Multifocus optical-resolution photoacoustic microscopy using stimulated Raman scattering and chromatic aberration," *Opt. Lett.* **38**(15), 2711–2713 (2013).

9. T. Buma, B. C. Wilkinson, and T. C. Sheehan, "Near-infrared spectroscopic photoacoustic microscopy using a multi-color fiber laser source," *Biomed. Opt. Express* **6**(8), 2819–2829 (2015).

10. L. Wang et al., "Fast voice-coil scanning optical-resolution photoacoustic microscopy," *Opt. Lett.* **36**(2), 139–141 (2011).

11. L. Li et al., "Fully motorized optical-resolution photoacoustic microscopy," *Opt. Lett.* **39**(7), 2117–2120 (2014).

12. Y. Wang and R. K. Wang, "Measurement of particle concentration in flow by statistical analyses of optical coherence tomography signals," *Opt. Lett.* **36**(11), 2143–2145 (2011).

13. S.-L. Chen et al., "Photoacoustic correlation spectroscopy and its application to low-speed flow measurement," *Opt. Lett.* **35**(8), 1200–1202 (2010).

14. B. Ning et al., "Simultaneous photoacoustic microscopy of microvascular anatomy, oxygen saturation, and blood flow," *Opt. Lett.* **40**(6), 910 (2015).

15. Y. Zhou et al., "Calibration-free absolute quantification of particle concentration by statistical analyses of photoacoustic signals in vivo," *J. Biomed. Opt.* **19**(3), 037001 (2014).

16. H. F. Zhang et al., "Imaging of hemoglobin oxygen saturation variations in single vessels in vivo using photoacoustic microscopy," *Appl. Phys. Lett.* **90**(5), 053901 (2007).

17. W. J. Smith, *Modern Optical Engineering: The Design of Optical Systems*, 4th ed., McGraw Hill, New York (2008).

18. J. Yao et al., "In vivo photoacoustic imaging of transverse blood flow by using Doppler broadening of bandwidth," *Opt. Lett.* **35**(9), 1419–1421 (2010).

19. C. Zhang et al., "In vivo photoacoustic microscopy with 7.6-μm axial resolution using a commercial 125-MHz ultrasonic transducer," *J. Biomed. Opt.* **17**, 116016 (2012).

20. T. Wang et al., "All-optical photoacoustic microscopy based on plasmonic detection of broadband ultrasound," *Appl. Phys. Lett.* **107**(15), 153702 (2015).

Tianxiong Wang received his BS degree in physics from the University of Science and Technology of China, Hefei, China, in 2010. Currently, he is a PhD student in the Department of Biomedical Engineering at the University of Virginia. His research focuses on the development of all-optical ultrasonic detectors and high-speed photoacoustic microscopy.

Naidi Sun received his BS and MS degrees in physical electronics from Harbin Institute of Technology in 2010 and 2012, respectively. Currently, he is a graduate student in the Department of Biomedical Engineering at the University of Virginia. His research focuses on the development of quantitative photoacoustic microscopy and its applications in brain imaging.

Rui Cao received his BS and MS degrees from Nankai University, Tianjin, China, in 2010 and 2013, respectively. Currently, he is a PhD student in the Department of Biomedical Engineering at the University of Virginia. His research focuses on multispectral photoacoustic microscopy, molecular photoacoustic imaging, and multimodal optical microscopy.

Bo Ning received his BS and PhD degrees in electronics science from Peking University, Beijing, China, in 2008 and 2013, respectively. Currently, he is a postdoctoral research associate in the Department of Biomedical Engineering at the University of Virginia. His research focuses on the development and application of multiparametric photoacoustic microscopy.

Ruimin Chen received his BS degree from the University of Electronics Science and Technology of China, Chengdu, China in 2006 and his PhD degree from the University of Southern California, Los Angeles, California in 2014. He is currently a research associate in the NIH Resource Center for Medical Ultrasonic Transducer Technology of University of Southern California. His research interests include high-frequency ultrasonic transducers and arrays for medical imaging applications, piezoelectric material characterization, and photoacoustic imaging.

Qifa Zhou received his PhD from Xi'an Jiaotong University, Xi'an, China in 1993. He is currently a professor of biomedical engineering, ophthalmology, and the NIH Resource Center for Medical Ultrasonic Transducer Technology at the University of Southern California, Los Angeles, California. His research interests include the development of piezoelectric high-frequency ultrasonic transducers for photoacoustic imaging, intravascular imaging and cell-tissue imaging.

Song Hu received his BS and MS degrees in electronic engineering from Tsinghua University, Beijing, China, in 2002 and 2005, respectively. He received his PhD in biomedical engineering from Washington University in St. Louis in 2010. Currently, he is an assistant professor of biomedical engineering in the University of Virginia. His research focuses on the development and application of photoacoustic microscopy in neuroscience, cancer, and cardiovascular diseases.